

www.advmattechnol.de

# A Programmable and Automated Platform for Integrated Synthesis and Evaluation of Water Electrolysis Catalysts

Changcheng Yu, Qi Xiong, Kai Yang, Haibiao Chen,\* and Feng Pan\*

A programmable and fully automated platform is created to take over tedious manual operations in a typical catalyst development process. Synthesis and evaluation of the catalyst are coupled as an operation unit to enable continuous and unattended execution of combinatorial experiments. This platform is demonstrated in the identification of high-performance bifunctional catalysts for water splitting from a trimetallic NiFeCo hydroxide system. The platform collects data for evaluating the performance of 66 different catalysts in oxygen evolution and hydrogen evolution reactions within a timeframe of four days. Timely feedback from the close-coupled evaluation enables a guided focused-area scanning of the parameter matrix, achieving both full coverage and a fine-tuned hit with a relatively smaller number of experiments. The optimal compositions of the catalysts identified by the platform are well consistent with previous reports. Therefore, the platform is capable of generating useful data for catalyst screening, allowing a researcher to focus more on creative tasks.

Catalysis is a surface phenomenon, and the catalytic performance of a material is closely related to the crystal structure and the electronic configurations of the surface. It is a common strategy to combine multiple elements to tailor the surface structure and electronic configuration to achieve high catalytic performance. The traditional process to develop a heterogeneous catalyst is lengthy and it can be labor-intensive to identify the optimal composition in a multiple-element system using a trial-and-error approach. In recent years, materials design based on computational simulation has become a powerful tool in predicting high-performance catalysts and help to reduce the number of experiments.<sup>[1]</sup> On the other hand, lab automation and high throughput experiment protocols further eliminate unnecessary laborious work and accelerate materials discovery.<sup>[2]</sup> Since its birth in the 1960s, combinatorial chemistry has become a mature research tool and the concept has been

C. Yu, Q. Xiong, K. Yang, Prof. H. Chen, Prof. F. Pan School of Advanced Materials Peking University Shenzhen Graduate School Shenzhen 518055, P. R. China E-mail: chenhb@pkusz.edu.cn, chenhb@szpt.edu.cn; panfeng@pkusz.edu.cn Prof. H. Chen Shenzhen Polytechnic Institute of Marine Biomedicine Shenzhen 518055, P. R. China

The ORCID identification number(s) for the author(s) of this article can be found under https://doi.org/10.1002/admt.202001036.

DOI: 10.1002/admt.202001036

adapted to materials science since 1990s.[3] In a typical procedure, a materials library containing a 2-D array of specimens with different compositions is prepared on a single substrate, and the response of each specimen is measured when an optical or electrical probe scans through the library. The combinatorial approach has been widely applied to catalyst development, especially for photocatalysts and electrocatalysts. [2b-f,4] The materials library is typically prepared by vacuum coating,[2g,3a,4c] inkjet printing,[2b,c,e,4b] diffusion couple, [2a] and electrodeposition. [2d,4a,5] In these prior works, however, the synthesis and the evaluation steps were usually separate by one or more steps requiring manual operation. For example, the materials library needs to be transferred to a furnace for calcination, and

then transferred to the high-throughput screening station. Also, both synthesis and evaluation are done in a batch manner that the feedback from the evaluation can only be used for the next batch. The strength of a human researcher is that he or she can modify the next specimen accordingly based on the evaluation result of the previous specimen. It is reasonable to integrate the synthesis and evaluation into a fully automated workflow to enable timely feedback during a series of experiments. In a new era of materials development, data becomes the only important object and the essential task of a researcher is to handle data of various types such as experimental parameters and results. The key to achieving this goal is to develop new tools to do all the dirty works using evolving computerized technologies and robots. At a high level of automation, advanced algorithms and artificial intelligence can even interpret natural languages to execute actual experiments, optimize parameters, and take over some planning of the experiments.<sup>[6]</sup> An additional benefit of using a machine to run the experiment is that all operations can be easily documented and traced, and in many cases, a machine performs better than a human in terms of precision and reproducibility.

The aim of our work is to develop a programmable platform to automate a typical process of electrocatalyst development. The platform is designed to carry out the synthesis and the subsequent evaluation of the electrochemical performance of the catalyst without human intervention. The major task of the user is to design the experiments, and then the platform will execute the experiments and generate data unattended  $24 \times 7$ . The user only has to focus on data analysis and experiment design, without having to perform any routine and repetitive lab work.

2365709x, 2021, 3, Downloaded

onlinelibrary.wiley.com/doi/10.1002/admt.202001036 by University Town Of Shenzhen, Wiley Online Library on [26/11/2025]. See the Terms and Conditions

and-conditions) on Wiley Online Library for rules of use; OA articles are governed by the applicable Creative Commons

Figure 1. A) Conceptional data-in/data-out structure of the automated platform; B) Main window of "HTPSolutions" program showing a diagram of the components in the platform for NiFeCo hydroxide based catalyst for water electrolysis; C) Actual hardware implementation of the platform.

Unlike other platforms, the user of this platform is not expected to know a programming language, and can easily program the platform using interactive interfaces. We anticipate that this platform can be further used to facilitate catalyst development process in general.

As shown in **Figure 1**A, a conceptional structure of the platform is to implement a data-in/data-out "black box". The input is a json-format experimental program containing a sequence of steps and an associated parameter matrix, and the output contains raw and processed data for visual examination of the catalytic performance. At the center of this black box, there is a computer running our "HTPSolutions" program that parses the user-input experimental program to the actual execution of the steps including: actuating the diluters to prepare solutions in a mixing container; transferring liquid from the mixing container to the reactor; triggering a potentiostat to run common electrochemical procedures; flushing the flow paths and containers after each individual experiment. In our setting, a materials library is not synthesized batch-wise and then evaluated batch-wise. Instead, an electrochemical evaluation of the performance can immediately follow the synthesis of a composition by electrodeposition. Synthesis and evaluation are coupled as an operation unit that walks through the virtual materials library. Potentially, an optimal parameter set can be located by taking a shortcut guided by an advanced algorithm, without having to iterate the whole library (Figure S1, Supporting Information).

For demonstration, a trimetallic system, NiFeCo hydroxide, was selected as the model catalyst and its performance in water electrolysis was evaluated. NiFe binary hydroxide is a proven catalyst for oxygen evolution reaction (OER) in basic media and has been studied for decades. Recently, NiFeCo

hydroxides were also explored as a bifunctional catalyst in water splitting since they can also catalyze the hydrogen evolution reaction (HER).<sup>[8]</sup> We can easily compare our results to widely available existing data to validate our platform. It has been verified that NiFeCo hydroxides as prepared by electrodeposition are partially crystalline and catalytically active in OER without heat treatment. In this work, NiFeCo hydroxides were prepared using an electrodeposition approach, and their performance in OER and HER was quantified by deriving the overpotentials and Tafel slopes from the linear sweep voltammetry (LSV) data.

A schematic diagram of the platform for the synthesis and evaluation of NiFeCo hydroxide catalysts is shown in Figure 1B, and the hardware implementation is shown in Figure 1C. The platform was built from commonly available structural parts, liquid handling equipment, and electronic components. The platform has a small footprint of only 60 cm × 60 cm and the total cost was approximately \$10 220 including the computer and the potentiostat (Table S1, Supporting Information). The platform contains three major modules: solution preparation, transfer and flush, and electrochemistry. Currently, the solution preparation module contains eight diluter channels which withdraw concentrates of chemicals and de-ionized water from the reservoirs and dispense them into the mixing container to prepare a solution of a specified concentration. Custom-built syringe pumps were used to drive the diluters because they can deliver liquids with high precision. Here, concentrated solutions include 0.5 M Ni(NO<sub>3</sub>)<sub>2</sub>, 0.5 M Fe(NO<sub>3</sub>)<sub>3</sub>, 0.5 M Co(NO<sub>3</sub>)<sub>2</sub>, 10 м KOH, and 5 м HNO<sub>3</sub>. Preparation and replenishment of the concentrates are the only few infrequent operations that still need to be done manually. Mixing and reaction take place

2365709x, 2021, 3, Downloaded from https://advanced.onlinelibrary.wiley.com/doi/10.1002/admt.202001036 by University Town Of Shenzhen, Wiley Online Library on [26/1/2025]. See the Terms

of use; OA articles are governed by the applicable Creative Commons License

separately in two 100 mL polyethylene containers, and liquid can be transferred from the mixing container to the reactor. Both the mixing and the reactor containers can be emptied and flushed clean after each individual experiment. Liquid transfer and flushing are controlled by coordinating the running of three peristaltic pumps, which can deliver a high flow rate. The electrochemistry module contains the reactor and a potentiostat. The reactor was equipped with a piece of  $1 \times 1 \, \mathrm{cm^2}$  carbon fiber paper (CFP) as the working electrode, Ag/AgCl (saturated KCl, 0.197 V versus reversible hydrogen electrode) as the reference electrode, and a graphite rod as the counter electrode.

To program a single experiment, a sequence of steps was entered by the user using an interactive step editor in the "HTPSolutions" program (Figure S2A, Supporting Information). Each step can be one of the five types of operations including: blank; solution preparation; transfer; flush; and electrochemistry. The steps designed for this work are shown as pseudocodes in Figure 2B. A program for combinatorial experiments can be run by associating a parameter matrix with the steps. To populate the parameter matrix with values, the user designates the starting value, the end value, and the increment for each parameter using an interactive interface (Figure S2B, Supporting Information). Numerical parameters including ion concentrations, electrical parameters, and time can be systematically varied and evaluated in combinatorial experiments. For an initial scan of the composition matrix, the concentrations of Ni, Fe, and Co were all varied from 0 to 0.1 м at an increment of 0.01 M, with the concentrations of all metal ions summing up to be 0.1 m. There were a total of 66 sets of parameters which include evenly spaced concentrations for each metal. The combinatorial experiments containing these 66 different parameter sets were run and completed in 90 h and 34 min. Every single experiment took an average of 82 min to complete, and the small variation in the duration came from the solution preparation step. The platform performing different steps in action

can be viewed in the supplementary videos. Every single experiment produced five data files including one *i-t* (current-time) curve, two cyclic voltammetry (CV) curves, and two LSV curves.

During the potentiostatic experiment in step #4 in Figure 2B. the applied potential drove HER at the working electrode and NiFeCo hydroxides were deposited onto the CFP substrate where OH- was generated from HER. If assuming all transferred electrons went to OH- and all OH- formed hydroxides matching the stoichiometry of the source solution, the average mass loading of the deposited catalyst would be 0.77 mg by integrating the i-t curves in Figure S3A, Supporting Information. However, the assumptions we made for the calculation can be erroneous because there could be other side reactions besides HER during our potentiostatic deposition. Not all OH- reacted with metal to form precipitates attaching to the working electrode. Also, Fe<sup>3+</sup> might be reduced to Fe<sup>2+</sup> and consume electrons in this process since Fe<sup>2+</sup> species were identified in the deposit as revealed by X-ray photoelectron spectroscopy (XPS, Figure S4, Supporting Information). Therefore, the calculated mass loading was only good for a very rough estimate. At the end of each experiment, the deposited catalyst was removed by electrochemical dissolution in step #15. Since catalysis is a surface-sensitive process, the substrate surface needs to as clean as possible to start. After running the dissolution process on a representative deposited catalyst Ni<sub>0.4</sub>Fe<sub>0.3</sub>Co<sub>0.3</sub>(OH)<sub>x</sub> for different lengths of durations, it was found that after 10-min dissolution there was no Ni<sup>2+</sup> oxidation peak or higher activity than the blank in the following LSV test on the substrate as shown in Figure S5, Supporting Information. We assumed that the effect from the previous sample was negligible on the next sample.

The CV curves prior to the OER and HER LSVs are shown in Figures S6 and S7, Supporting Information. Common in all curves is that the first cycle is very different from the rest, and after the first cycle the curves gradually overlap. The result justified the necessity of CV scans for stabilizing the surface

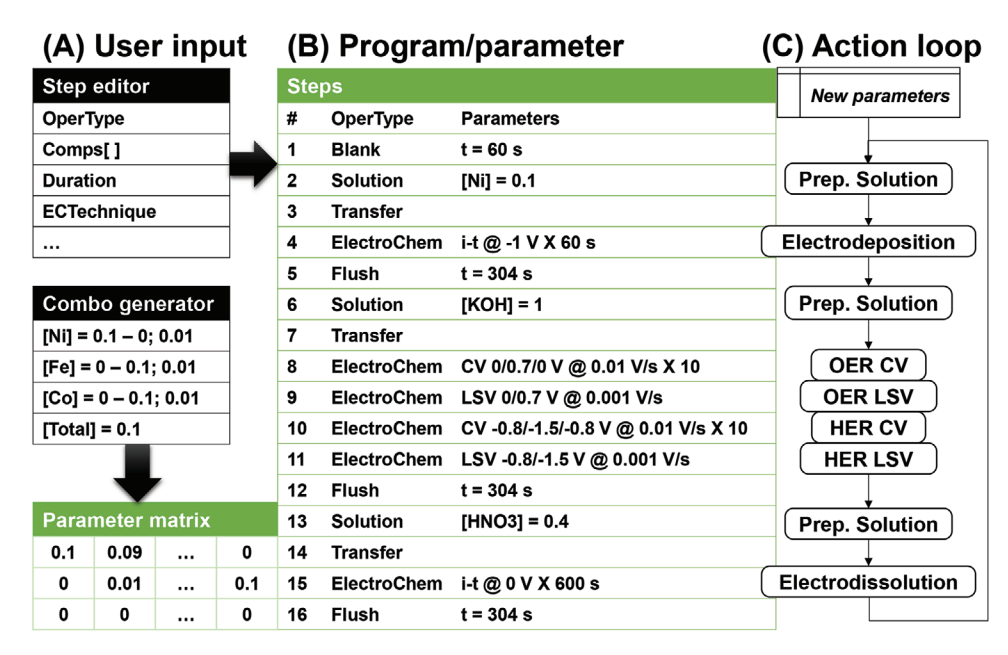


Figure 2. A) Step editor generates B) a sequence of steps, and a parameter generator populates the parameter matrix associated with the steps in (B) by a user-input range of values and increments. C) Action loop performed by the platform to execute the experiments and iterate the parameter matrix.

2365709x, 2021, 3, Downloaded from https://advanced.onlinelibrary.wiley.com/doi/10.1002/admt.202001036 by University Town Of Shenzhen, Wiley Online Library on [26/11/2025]. See the Terms and Conditions (https://doi.org/10.1002/admt.202001036 by University Town Of Shenzhen, Wiley Online Library on [26/11/2025]. See the Terms and Conditions (https://doi.org/10.1002/admt.202001036 by University Town Of Shenzhen, Wiley Online Library on [26/11/2025]. See the Terms and Conditions (https://doi.org/10.1002/admt.202001036 by University Town Of Shenzhen, Wiley Online Library on [26/11/2025]. See the Terms and Conditions (https://doi.org/10.1002/admt.202001036 by University Town Of Shenzhen, Wiley Online Library on [26/11/2025]. See the Terms and Conditions (https://doi.org/10.1002/admt.202001036 by University Town Of Shenzhen, Wiley Online Library on [26/11/2025].

of use; OA articles are governed by the applicable Creative Commons License

www.advancedsciencenews.com

www.advmattechnol.de

structure before the actual performance test. The reversible redox peaks for  $Ni^{2+} \Leftrightarrow Ni^{3+}$  (Ni(OH)<sub>2</sub>  $\Leftrightarrow$  NiOOH) are visible in the OER CV scans. For pure Ni(OH)2, the oxidation peak is at around 1.37 V. The effect of Fe and Co on the position of the Ni redox peak can be easily identified from the CV curve of the 5th cycle as shown in Figure S8, Supporting Information. For the NiFe binary hydroxide, the redox peaks gradually shifted towards the positive direction as the Fe content increased. For the NiCo binary hydroxide, the redox peaks gradually shifted towards the negative potential as the Co content increased. Consistent shifts of the redox peaks in CVs for Ni<sup>2+</sup> were also observed in previous works and they can be attributed to the distinct electron push and pull effects of Co and Fe imposing on Ni which. [7,8b] Fe3+ tends to pull electrons away from Ni2+, and the catalyst as a whole binds the active electrons more tightly therefore it is more difficult to extract electrons from the surface using an external bias, leading to a higher oxidation potential. The effect of Co<sup>2+</sup> is just the opposite. The electronic push and pull effects of Co and Fe on Ni were elucidated in detail in our previous work, by performing XPS analysis on the Ni 2p and O 1s spectra and theoretical calculation of the binding energies of adsorbed species.<sup>[8b]</sup> The consistent shifts of the redox peak position as the Fe/Co concentration changed verified that the platform was able to produce reasonable data unattended, and that it is possible to tune the electrochemical behavior by varying the composition of the trimetallic hydroxide.

The OER and HER performance of each catalyst were evaluated by identifying the overpotential at a current density of 10 mA cm<sup>-2</sup> ( $\eta_{10}$ ) and the Tafel slope from the corresponding LSV data in Figure S9, Supporting Information. The dependences of the figures of merit on the composition are summarized in **Figure 3** and Tables S3–S6, Supporting Information. From the OER LSV curves, we can also identify the oxidation of Ni<sup>2+</sup> to Ni<sup>3+</sup>. However, the intensity of the peak is much weaker in LSV than in CV because in LSV the scan rate was reduced by an order of magnitude. From the ternary plot of  $\eta_{10}$  in Figure 3A, catalyst Ni<sub>0.7</sub>Fe<sub>0.3</sub>(OH)<sub>x</sub> achieved the lowest  $\eta_{10}$  of only 240 mV. A general trend can be observed that  $\eta_{10}$  was lower when the composition is closer to the Ni-Fe edge excluding

vertexes representing pure Ni and Fe. The initial combinatorial experiment used a step size of 0.1 in the normalized concentration of the metal ions. Fine tuning of the composition can be done at a smaller step size. With the feedback from the initial scan, a triangular region enclosing the Ni<sub>0.7</sub>Fe<sub>0.3</sub>(OH)<sub>x</sub> composition with the normalized concentration of Ni in the range from 0.55 to 0.85, Fe in the range from 0.15 to 0.45, and Co in the range from 0 to 0.3 was scanned at a smaller step size of 0.03. The results of these 66 experiments are plotted in Figure 3B. For an easy comparison, the ternary plots for the initial scan and the focused-area scan are prepared using the same color scale (Figure S11, Supporting Information). There are some duplicated compositions in the two scans and the variation of  $\eta_{10}$  is within 5%. The combination of an initial scan and a focused-area scan can cover the full parametric space and still can locate a composition with high precision without testing as many samples. For example, if the composition library is to be scanned evenly using a step size of 0.03, there will be a total of 561 experiments to run. By combining an initial scan and a fine scan, we can achieve the same level of precision by running only 66 + 66 = 132 experiments, which accounted for only one fourth of the number of experiments in a uniform scan. This strategy demonstrated the agility of the in situ planning guided by timely feedback in comparison to the traditional high-throughput approach.

In the fine scan, the composition with the lowest  $\eta_{10}$  of 233 mV turned out to be Ni<sub>0.67</sub>Fe<sub>0.33</sub>(OH)<sub>x</sub>, which is very close to composition Ni<sub>0.7</sub>Fe<sub>0.3</sub>(OH)<sub>x</sub> and this composition is also on the Ni-Fe edge. As another figure of merit, the Tafel slope did not show a clear trend in the initial scan. Since during LSV, the surface reaction is not at steady-state, it has been suggested that getting Tafel slope from a chronopotentiometry or a chronoamperometry method is more reliable. To verify that whether the Tafel slope overturned the trend in the overpotential at a higher current density, the overpotentials at 50 mA cm<sup>-2</sup> ( $\eta_{50}$ ) were examined from all LSV curves from the initial scan and the values were plotted in another ternary graph shown in Figure S11, Supporting Information. Still, Ni<sub>0.7</sub>Fe<sub>0.3</sub>(OH)<sub>x</sub> catalyst showed the lowest overpotential of 268 mV at this current

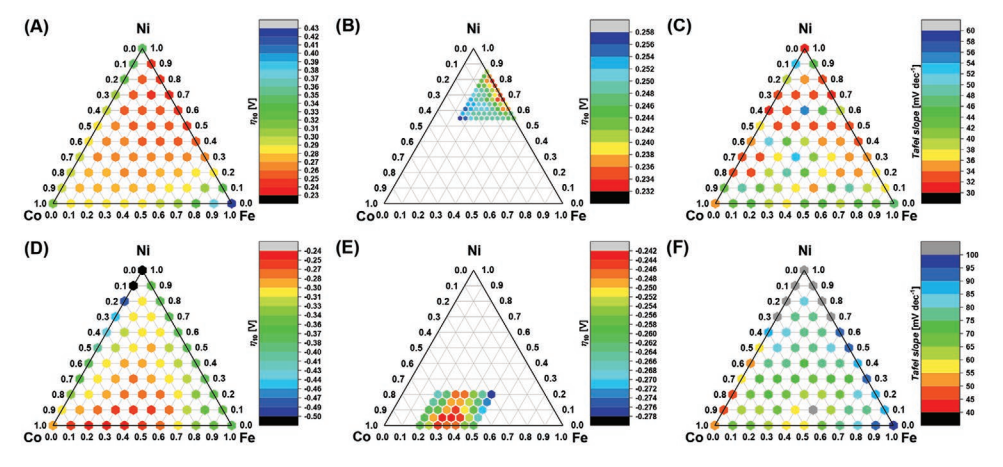


**Figure 3.** Ternary plots of figures of merit obtained from the LSV curves: A) OER overpotential at 10 mA cm<sup>-2</sup> (full-range scan of the compositional matrix); B) OER overpotential at 10 mA cm<sup>-2</sup> (focused scan of the high-performance area); C) OER Tafel slope (full-range scan); D) HER overpotential at 10 mA cm<sup>-2</sup> (focused area scan); F) HER Tafel slope (full-range scan). Note: Ternary plots are based on the composition of the solution used for electrodeposition, not the actual composition of the catalyst.

ADVANCED MATERIALS TECHNOLOGIES 23657992, 2021, 3, Downloaded from https://dvanced.onlinelibtrary.wiley.com/oi/10/10/20/attenced.onlinelibtrary.wiley.com/oi/10/20/attenced.onlinelibtrary.wiley.com/oi/10/20/attenced.onlinelibtrary.wiley.com/oi/10/20/attenced.onlinelibtrary.wiley.com/oi/10/20/attenced.onlinelibtrary.wiley.com/oi/10/20/attenced.onlinelibtrary.wiley.com/oi/10/20/attenced.onlinelibtrary.wiley.com/oi/10/20/attenced.onlinelibtrary.wiley.com/oi/10/20/attenced.onlinelibtrary.wiley.com/oi/10/20/attenced.onlinelibtrary.wiley.com/oi/10/20/attenced.onlinelibtrary.wiley.com/oi/10/20/attenced.onlinelibtrary.wiley.com/oi/10/20/attenced.onlinelibtrary.wiley.com/oi/10/20/attenced.onlinelibtrary.wiley.com/oi/10/20/attenced.onlinelibtrary.wiley.com/oi/10/20/attenced.onlinelibtrary.wiley.com/oi/10/20/attenced.onlinelibtrary.wiley.com/oi/10/20/attenced.onlinelibtrary.wiley.c

density. Similar treatment was applied to the fine-scan region while another benchmark current density at 100 mA cm $^{-2}$  was considered. The lowest overpotential at 100 mA cm $^{-2}$  ( $\eta_{100}$ ) was 293 mV, also from catalyst Ni $_{0.67}$ Fe $_{0.33}$ (OH) $_x$ . Analyses of the OER data lead to a consistent conclusion that Ni $_{0.67}$ Fe $_{0.33}$ (OH) $_x$  is the best OER catalyst for the compositions evaluated. The dependence of the OER performance on the composition of the NiFeCo hydroxides agrees well with previous studies, and the  $\eta_{10}$  of the optimal catalyst is comparable to the state-of-the-art multielement OER catalysts, for example, 310 mV for Ni $_{0.2}$ Co $_{0.3}$ Ce $_{0.5}$ O $_x$ , 272 mV for (Co $_{0.21}$ Ni $_{0.25}$ Cu $_{0.54}$ ) $_3$ Se $_2$ , 230 mV for (Ni $_{0.25}$ Fe $_{0.68}$ Co $_{0.07}$ ) $_3$ Se $_4$ , and 239 mV for Ni $_{0.8}$ Co $_{0.1}$ Fe $_{0.1}$ O $_x$ H $_y$ [<sup>2lb.c.4a,5,8b,9]</sup>

Similar analyses were applied to the HER LSV data. In the initial scan, Fe<sub>0.3</sub>Co<sub>0.7</sub>(OH)<sub>x</sub> was identified to show the lowest  $\eta_{10}$  of 245 mV while Fe<sub>0.4</sub>Co<sub>0.6</sub>(OH)<sub>x</sub> showed the lowest  $\eta_{50}$ of 289 mV. A fine scan was performed in a region enclosing these compositions with the normalized concentration of Ni from 0 to 0.2, Fe from 0.2 to 0.5, Co from 0.3 to 0.8, with a step size of 0.05. The shape of the scanned area is a parallelogram and there are 35 compositions in this region. Interestingly, the fine scan identified Ni<sub>0.05</sub>Fe<sub>0.35</sub>Co<sub>0.6</sub>(OH)<sub>x</sub> as the best catalyst with a low  $\eta_{10}$  of 242 mV, suggesting that a small amount of Ni may promote the activity although a high content of Ni generally causes an adverse effect. For an easy comparison, the ternary plots for the initial scan and the focused-area scan are prepared using the same color scale (Figure S12, Supporting Information). There are some duplicated compositions in the two scans and the variation of  $\eta_{10}$  is within 10%. The trend shown in the ternary plot for the Tafel slope is different from the overpotential plot. The ternary plots of the Tafel slope suggest that Co facilitates a fast electron transfer while Ni hinders it. Note that the comparison of the overpotential at a specific geometrical current density reflects the macroscale behavior and not necessarily represents the intrinsic activity, but this figure of merit is more relevant in real-life applications. In practical applications, a low overpotential at a high current density is essential for the economy. We further compared the overpotentials of the HER catalysts in the fine scan at a current density of 100 mA cm<sup>-2</sup> (Figure S13, Supporting Information). For HER, the lowest  $\eta_{100}$ of 326 mV was found in catalyst Ni<sub>0.2</sub>Fe<sub>0.35</sub>Co<sub>0.45</sub>(OH)<sub>x</sub>. For comparison, the aforementioned  $Ni_{0.05}Fe_{0.35}Co_{0.6}(OH)_x$  exhibited a similar  $\eta_{100}$  of 329 mV at this current density. The difference is quite small, and Ni<sub>0.05</sub>Fe<sub>0.35</sub>Co<sub>0.6</sub>(OH)<sub>x</sub> performed better in the whole current density range overall. However, the unexpectedly high performance of Ni<sub>0.2</sub>Fe<sub>0.35</sub>Co<sub>0.45</sub>(OH)<sub>x</sub> at a high current density requires more investigations in the future.

Chemical and structural analyses were carried out ex situ on two catalysts showing promising results, which are  $Ni_{0.67}Fe_{0.33}(OH)_x$  for OER and  $Ni_{0.05}Fe_{0.35}Co_{0.6}(OH)_x$  for HER, respectively. Inductively coupled plasma atomic emission spectroscopy (ICP-AES) measured the actual compositions of  $Ni_{0.67}Fe_{0.33}(OH)_x$  and  $Ni_{0.05}Fe_{0.35}Co_{0.6}(OH)_x$  to be  $Ni_{0.42}Fe_{0.58}(OH)_x$  and  $Ni_{0.03}Fe_{0.55}Co_{0.42}(OH)_x$ , respectively. Apparently, during the co-deposition process, Fe is preferentially deposited and the mole fraction of Fe is higher in the deposits than in the solution. To verify the trend, two additional samples were measured. The actual composition of  $Ni_{0.33}Fe_{0.33}Co_{0.33}(OH)_x$  was measured to be  $Ni_{0.22}Fe_{0.50}Co_{0.28}(OH)_x$ , and the composition of  $Ni_{0.10}Fe_{0.80}Co_{0.10}(OH)_x$  was measured to be

Ni<sub>0.06</sub>Fe<sub>0.88</sub>Co<sub>0.06</sub>(OH)<sub>x</sub>. Although the composition of a deposit deviated from that of the solution, the trend was consistent and it enables the control of the composition of the deposit. Obtained from the ICP-AES data, the mass loadings of  $Ni_{0.67}Fe_{0.33}(OH)_x$ ,  $Ni_{0.05}Fe_{0.35}Co_{0.6}(OH)_x$ ,  $Ni_{0.33}Fe_{0.33}Co_{0.33}(OH)_x$ , and  $Ni_{0.10}Fe_{0.80}Co_{0.10}(OH)_x$  were 0.61, 0.51, 0.69, and 0.32 mg, respectively. The measured mass loading was lower than the value calculated from the i-t curve. The discrepancy might be caused by the side reactions during the deposition process and hydroxide precipitates not attaching to the substrate. The surface morphologies of the Ni<sub>0.67</sub>Fe<sub>0.33</sub>(OH)<sub>x</sub> and Ni<sub>0.05</sub>Fe<sub>0.35</sub>Co<sub>0.6</sub>(OH)<sub>x</sub> catalysts were observed by scanning electron microscopy (SEM) and the images are shown in Figure 4. The structure of  $Ni_{0.67}Fe_{0.33}(OH)_x$  appears to be cellular with thin walls, quite similar to the structures previously reported for the electrodeposited NiFe catalysts. [5,8b,10] The deposited Ni<sub>0.05</sub>Fe<sub>0.35</sub>Co<sub>0.6</sub>(OH)<sub>x</sub> catalyst was composed of nodules with a diameter of about 200 nm, resembling typical electrodeposited porous structures.<sup>[8b]</sup> The phase of the selected catalysts was identified using X-ray diffraction (XRD). As shown in Figure S14, Supporting Information, both diffraction patterns of  $Ni_{0.67}Fe_{0.33}(OH)_x$  and  $Ni_{0.05}Fe_{0.35}Co_{0.6}(OH)_x$  were found to match well with  $\alpha$ -Ni(OH)<sub>2</sub>, suggesting that these catalysts have a layered double hydroxide (LDH) structure.

In this work, the deposited catalyst was electrochemically dissolved after each experiment and the CFP substrate was reused. It was a concern that there could be a trace amount of residue that would affect the result of the following experiments. To address this concern, the same set of experiments was run by iterating the parameter matrix in a reversed order, and the results are shown in the ternary plots (Figure S15, Supporting Information). It can be observed that regardless of the scanning path, the dependences of the overpotential and Tafel slope on the composition are unaltered. Therefore, even if there was residue after the electrochemical dissolution, either the amount of the residue was negligible or the residue was completely covered by the following deposits, and thus the residue did not affect the result noticeably.

In summary, a programmable and automated platform for the synthesis and evaluation of electrocatalyst was built and demonstrated. The platform carried out routine experimental operations for catalyst development unattended and continuously. Using NiFeCo hydroxide as a model, the platform demonstrated that the data can be generated quickly and the optimal catalysts can be easily identified from a parameter matrix of compositions. The data from the automated platform agreed very well with previous reports. Instead of synthesizing and evaluating a complete materials library batch-wise, our automated platform simulated a human researcher and produced timely feedback from each experiment during the search of optimal parameters. The close coupling of the synthesis-evaluation cycle can reduce the number of experiments. More importantly, the enclosed and completely automated experimental cycle enables a data-driven machine for materials development where the inputs and outputs can be digitally transferred, processed, and shared.

Certainly, here we are only showing a prototype of the platform which is being constantly improved and upgraded. Several features will be integrated into future versions. First, a fresh substrate will be used for each experiment to avoid

Figure 4. A,B): SEM image of Ni<sub>0.67</sub>Fe<sub>0.33</sub>(OH)<sub>x</sub>; C,D): SEM image of Ni<sub>0.05</sub>Fe<sub>0.35</sub>Co<sub>0.6</sub>(OH)<sub>x</sub>.

contamination between samples and a three-axis positioning stage will be integrated to handle the substrates in an array. Second, parallel processing will be introduced to overlap experiments at different steps to further improve the efficiency and fully utilize the hardware resource. Third, advanced algorithms will be developed to automatically determine the path through the parameter matrix in situ using fresh results, to obtain the optimal parameters quicker and reduce the number of experiments. Forth, the platform will be integrated with a gas control module and used for the development of catalysts for other important electrochemical reactions such as oxygen reduction, carbon dioxide reduction, and nitrogen reduction.

#### **Experimental Section**

Configuration of the Platform: The structural frame of the platform was built up using 2020 European Standard profile aluminum rails. The syringe pumps of the diluter channels were custom-made with microcontrollers that communicate with the computer via USB ports. The peristaltic pumps in the transfer and flush module were purchased from Baoding Signal Fluid Technology Co., Ltd. (Baoding, China) and multiple pumps were controlled via a single RS-485 bus. The RS-485 bus was connected to the computer via an LX08H USB-485 adapter (Road Number IoT Technology Co, Ltd., Foshan, China). The potentiostat of the electrochemistry module was a CHI660E unit purchased from CHI Instruments, Inc. (Shanghai, China).

An "HTPSolutions" program was developed using Visual C# to control the platform. The program provided interactive interfaces for entering an experimental program containing a list of steps and an associated parameter matrix. The syringe pumps and peristaltic pumps were controlled by the program using proprietary protocols defined by the device manufacturers. The program interoperated with the CHI660E potentiostat to run experiments and transfer data via a dynamic link library ("LibEC.dll") provided by the manufacturer.

Basic Experimental Program: The major steps in the basic experimental program shown in Figure 2B can be interpreted as follows: 1) A solution

containing 0.1 m Ni was prepared; 2) A potentiostatic experiment was conducted at  $-1\ V$  for 60 s to electrodeposit a metal hydroxide onto the CFP substrate; 3) A solution of 1 m KOH was prepared; 4) Five cycles of CV scans in the range from 0 to 0.7 at a scan rate of 0.01 V s $^{-1}$  were run to stabilize the structure of the deposited catalyst; 5) An LSV scan from 0 to 0.7 V at a scan rate of 0.001 V s $^{-1}$  was run to evaluate the OER performance; 6) Five cycles of CV scans in the range from  $-0.8\ \text{to}-1.5\ \text{V}$  at a scan rate of 0.01 V s $^{-1}$  were run to stabilize the catalyst; 7) An LSV scan from  $-0.8\ \text{to}-1.5\ \text{V}$  at a scan rate of 0.001 V s $^{-1}\ \text{was}$  was run to evaluate the HER performance; 8) A solution of 0.4 m HNO3 was prepared; 9) A potentiostatic experiment was conducted at 0 V for 600 s to accelerate the dissolution of the hydroxide on the substrate, and the substrate became ready for the next experiment.

Processing of Electrochemical Data: Depending on the types of electrochemical tests, values such as voltage, current, and time were recorded by the "HTPSolutions". These data were further processed by a Python script to obtain figures of merit, including overpotentials and Tafel slope, and generate graphs for visual evaluation by interacting with the Origin graphing software. The measured potentials in CV and LSV tests were compensated by the iR drop across the electrolyte. The overpotentials were calculated using the following equations:

$$\eta_{OER} = E_{Ag/AgCl} + 0.197V + 0.0591pH - 1.229V$$
(1)

$$\eta_{\text{HER}} = E_{\text{Ag/AgCI}} + 0.197\text{V} + 0.059\text{lpH}$$
(2)

Materials Characterizations: Metal contents of the deposited catalysts were analyzed using ICP-AES performed on a JY2000-2 (HORIBA Jobin Yvon, Japan) unit. SEM images were taken using a ZEISS Supra 55 microscope. XRD data were recorded using a Bruker D8 Advance diffractometer with Cu K $\alpha$  radiation of  $\lambda$  = 1.541 Å. XPS spectra were collected using an ESCALAB 250XL spectrometer.

### **Supporting Information**

Supporting Information is available from the Wiley Online Library or from the author.

www.advancedsciencenews.com

www.advmattechnol.de



2365709x, 2021, 3, Downloaded from https://advanced.onlinelibrary.wiley.com/doi/10.1002/admt.202001036 by University Town Of Shenzhen, Wiley Online Library on [26/1/2025]. See the Terms

of use; OA articles are governed by the applicable Creative Commons License

### Acknowledgements

C.Y. and Q.X. contributed equally to this work. This work was financially supported by the National Key Research and Development Program of China (2016YFB0700600) and Shenzhen Science and Technology Research Grant (JCY)20170818085823773).

#### **Conflict of Interest**

The authors declare no conflict of interest.

#### **Data Availability Statement**

Research data are not shared.

## **Keywords**

combinatorial experiments, electrocatalyst, lab automation, water splitting

Received: October 19, 2020 Revised: December 22, 2020 Published online: February 10, 2021

- B. Hinnemann, P. G. Moses, J. Bonde, K. P. Jørgensen, J. H. Nielsen, S. Horch, I. Chorkendorff, J. K. Nørskov, J. Am. Chem. Soc. 2005, 127, 5308.
- [2] a) T. Deng, T. Xing, M. Brod, Y. Sheng, P. Qiu, I. Veremchuk, Q. Song, T.-R. Wei, J. Yang, G. J. Snyder, Y. Grin, L. Chen, X. Shi, Energy Environ. Sci. 2020, 13, 3041; b) J. M. Gregoire, C. Xiang, X. Liu, M. Marcin, J. Jin, Rev. Sci. Instrum. 2013, 84, 024102; c) J. A. Haber, Y. Cai, S. Jung, C. Xiang, S. Mitrovic, J. Jin, A. T. Bell, J. M. Gregoire, Energy Environ. Sci. 2014, 7, 682; d) T. F. Jaramillo,

- S.-H. Baeck, A. Kleiman-Shwarsctein, K.-S. Choi, G. D. Stucky, E. W. McFarland, *J. Comb. Chem.* **2005**, *7*, 264; e) M. Woodhouse, G. S. Herman, B. A. Parkinson, *Chem. Mater.* **2005**, *17*, 4318; f) C. Xiang, S. K. Suram, J. A. Haber, D. W. Guevarra, E. Soedarmadji, J. Jin, J. M. Gregoire, *ACS Comb. Sci.* **2014**, *16*, 47; g) L. Zhou, A. Shinde, D. Guevarra, M. H. Richter, H. S. Stein, Y. Wang, P. F. Newhouse, K. A. Persson, J. M. Gregoire, *J. Mater. Chem. A* **2020**, *8*, 4239.
- [3] a) X.-D. Xiang, X. Sun, G. Briceno, Y. Lou, K.-A. Wang, H. Chang, W. G. Wallace-Freedman, S.-W. Chen, P. G. Schultz, *Science* 1995, 268, 1738; b) E. Reddington, *Science* 1998, 280, 1735.
- [4] a) X. Cao, E. Johnson, M. Nath, J. Mater. Chem. A 2019, 7, 9877; b) J. A. Haber, C. Xiang, D. Guevarra, S. Jung, J. Jin, J. M. Gregoire, ChemElectroChem 2014, 1, 524; c) C. Schwanke, H. S. Stein, L. Xi, K. Sliozberg, W. Schuhmann, A. Ludwig, K. M. Lange, Sci. Rep. 2017, 7, 44192
- [5] X. Cao, Y. Hong, N. Zhang, Q. Chen, J. Masud, M. A. Zaeem, M. Nath, ACS Catal. 2018, 8, 8273.
- [6] a) C. W. Coley, D. A. Thomas, J. A. M. Lummiss, J. N. Jaworski, C. P. Breen, V. Schultz, T. Hart, J. S. Fishman, L. Rogers, H. Gao, R. W. Hicklin, P. P. Plehiers, J. Byington, J. S. Piotti, W. H. Green, A. J. Hart, T. F. Jamison, K. F. Jensen, *Science* 2019, 365, eaax1566; b) S. Steiner, J. Wolf, S. Glatzel, A. Andreou, J. M. Granda, G. Keenan, T. Hinkley, G. Aragon-Camarasa, P. J. Kitson, D. Angelone, L. Cronin, *Science* 2019, 363, eaav2211; c) B. Burger, P. M. Maffettone, V. V. Gusev, C. M. Aitchison, Y. Bai, X. Wang, X. Li, B. M. Alston, B. Li, R. Clowes, N. Rankin, B. Harris, R. S. Sprick, A. I. Cooper, *Nature* 2020, 583, 237.
- [7] L. Trotochaud, S. L. Young, J. K. Ranney, S. W. Boettcher, J. Am. Chem. Soc. 2014, 136, 6744.
- [8] a) Q. Zhang, N. M. Bedford, J. Pan, X. Lu, R. Amal, Adv. Energy Mater. 2019, 9, 1901312; b) Q. Zhao, J. Yang, M. Liu, R. Wang, G. Zhang, H. Wang, H. Tang, C. Liu, Z. Mei, H. Chen, F. Pan, ACS Catal. 2018, 8, 5621; c) X. Zhu, C. Tang, H.-F. Wang, B.-Q. Li, Q. Zhang, C. Li, C. Yang, F. Wei, J. Mater. Chem. A 2016, 4, 7245.
- [9] R. D. L. Smith, M. S. Prévot, R. D. Fagan, S. Trudel, C. P. Berlinguette, J. Am. Chem. Soc. 2013, 135, 11580.
- [10] X. Lu, C. Zhao, Nat. Commun. 2015, 6, 6616.